THE JOURNAL OF PHYSICAL CHEMISTRY A
A JOURNAL OF THE AMERICAN CHEMICAL SOCIETY

pubs.acs.org/JPCA Article

# Linear and Helical Carbonic Acid Clusters

Austin M. Wallace and Ryan C. Fortenberry*

Cite This: J. Phys. Chem. A 2021, 125, 4589–4597 Read Online

ACCESS | Metrics & More | Article Recommendations

**ABSTRACT:** Crystallization of carbonic acid likely begins with a linear or ribbon-esque oligomerization, but a helical spiral is shown here to be a new, competing motif for this process. The present combined density functional theory and coupled-cluster theory work examines both the ribbon and the new helical spiral motifs in terms of relative energies, sequential binding energies, and electronic spectra which could potentially aid in distinguishing between the two forms. The helix diverges in energy from the ribbon by roughly 0.2 eV (~4 kcal/mol) per dimer addition, but the largest intensity absorption features at 9.16 eV (135 nm) and 7.11 eV (175 nm), respective of the ribbon and spiral, will allow these to be separately observed and classified via electronic spectroscopy to determine more conclusively which motif holds in the earliest formation stages of solid carbonic acid.

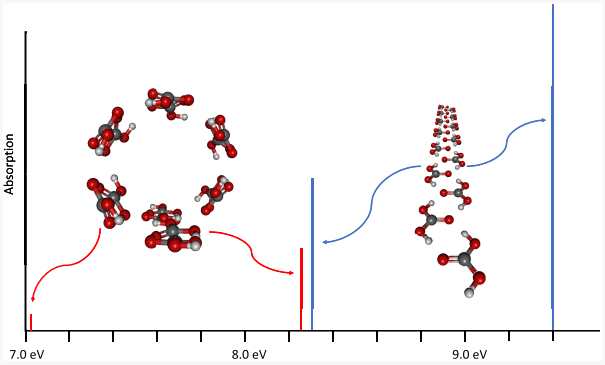




## INTRODUCTION

Carbonic acid is a simple organic molecule examined for numerous applications, but even such a simple, well-studied system can still have surprising properties. From its association with ocean acidification and $CO_2$ transport in blood, carbonic acid is prevalent on earth. However, it also plays roles in extraterrestrial environments, such as potentially on the surface of Mars with implications for both organic and inorganic chemistry.[1] Within the vacuum of space, carbonic acid may exist as ice especially since both $CO_2$ and water ices (as well as their mixture) are well-known,[2−5] but it has yet to be directly observed beyond the Earth.

Experimentally, trace amounts of carbonic acid have been produced through the irradiation of $H_2O$ and $CO_2$ ice (1:1) after slow warming from 20 K and identified through infrared spectroscopy at 215 K simulating various astrochemical conditions.[6] Solid carbonic acid has also been produced through acid−base reactions between HBr and $KHCO_3$ under vacuum at low temperature.[7] Ultimately, carbonic acid has been shown to form readily through ionizing radiation and vacuum−UV light on $H_2O$ + $CO_2$ ice.[8] As noted by Peeters and co-workers, both $H_2O$ and $CO_2$ have been found in the outer Solar System on satellites orbiting Jupiter, Saturn, Uranus, and Neptune.[7] These environments have radiation which can enable the formation of carbonic acid. However, detection of carbonic acid has yet remained elusive implying that any possible observations of this material might require it to exist in a solid, ice phase or as small clusters in the gas phase.

If it exists in space, solid carbonic acid is almost certainly in some largely, amorphous solid phase under interstellar or interplanetary conditions. However, smaller clusters may nucleate in motifs similar to bulk solids closer to STP. Carbonic acid was thought to reside in one of two solid phases, $\alpha$ and $\beta$, with the latter having received much more analytical scrutiny. The $\beta$ phase was thought to produce macroscopic tendrils when observed via microscopy, whereas the $\alpha$ phase produced clumps of material.[9−11] However, recent work with more advanced experimental techniques has shown that $\alpha$-carbonic acid is actually the monomethyl ester of carbonic acid and is not a polymorph negating the need for any further analysis of the $\alpha$ phase.[12] Even so, efforts to describe $\beta$-carbonic acid computationally have been successful in correlating with experiments for infrared and Raman spectra of a linear octamer.[13] Attempts to construct a crystal structure through molecular dynamic methods suggest that the crystals with "sheet-like hydrogen bonding topologies" are among the most stable.[14]

However, experimental characterization for nucleating solids from clusters of carbonic acid may require other spectroscopies that are more sensitive to structure than infrared or Raman techniques. Therefore, an exploration into the ultraviolet and visible spectra of small clusters of carbonic acid may provide more options for detecting carbonic acid and its isomers in

Received: March 30, 2021
Revised: May 7, 2021
Published: May 24, 2021

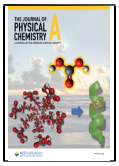





https://doi.org/10.1021/acs.jpca.1c02878
J. Phys. Chem. A 2021, 125, 4589−4597

outer Solar System environments and beyond. The present work will provide structural and electronic spectral characterization for associations of carbonic acid clusters.

## METHODS AND COMPUTATIONAL DETAILS

The present study focuses on computing the lowest energy structures for $n$-mers of carbonic acid for $n = 1 - 6$ with selected higher $n$ values. Additionally, excited states for the carbonic acid monomer, dimer, and some higher clusters of carbonic acid will also be explored. The geometry optimizations, energies, and harmonic zero-point vibrational energy corrections for the carbonic acid molecules are determined primarily by the $\omega$B97XD method with its long-range functionality[15,16] and the 6-31+G* basis set[17−20] both computed through Gaussian16.[21] This method and basis set are standard for computing clusters of molecules where intermolecular forces between molecules are necessary, like that for carbonic acid here, and $\omega$B97XD captures both short-range and long-range interactions more accurately than B3LYP.[22]

After optimizing the geometries, excited states are computed using time-dependent density functional theory (TD-DFT)[23,24] with the B3LYP method[25−27] and 6-311G*[28] basis set through Gaussian09. A more accurate calculation for excited states is accomplished for some clusters as noted in the discussion through equation-of-motion coupled-cluster theory at the singles and doubles level (EOM-CCSD)[29−31] run through Molpro[32] and the aug-cc-pVDZ basis set.[33,34] Although B3LYP is perceived not to be as systematically accurate as EOM-CCSD, B3LYP provides a less computationally expensive calculation for the larger carbonic acid systems. The present purpose is to determine excitation behavior changes as the structures become larger. Therefore, EOM-CCSD is used as a benchmark calculation on the monomer, dimer, and tetramer structures to indicate a subsequent energy value shift on the energies generated by the TD-DFT/B3LYP computations. The excited-state calculations provide spectral information for the isomers and increasing cluster sizes. The Kohn−Sham orbitals and molecular orbitals (MO) are plotted in the figures present in the next section, respectively, for the TD-DFT and EOM-CCSD calculations with the 6-311G*and aug-cc-pVDZ basis sets, respectively. These orbitals are investigated to examine the behavior of excitations within a series of increasing monomer units with the aim to establish a link between small carbonic acid systems and extrapolating to approximate bulk behavior.

## RESULTS AND DISCUSSION

**Structures.** The relative carbonic acid monomer energies are shown in Figure 1 with the most stable structure depicted on the far left. The *syn*−*syn* carbonic acid monomer (0.00 eV) is the lowest energy structure followed by the *syn*−*anti* (+0.08 eV, in line with previous computational results[9,35]) and then the *anti*−*anti* (+0.49 eV), according to the $\omega$ B97XD/6-31+G*. The *syn*−*syn* molecules have H−O−C *syn* angles that are 108.9° with the C−O, C═O, and O−H bonds being 1.333, 1.209, and 0.965 Å, respectively. The *syn*−*anti* molecule has one H−O−C *syn* angle at 107.4° with the associated C−O bond being 1.351 Å. The other H−O−C trans angle is 110° and has C−O and C═O bond distances of 1.333, and 1.199 Å. The *anti*−*anti* has two H−O−C down angles at 114.476° with the C−O, C═O, and O−H bond lengths of 1.352, 1.192, and 0.962 Å, respectively. These relative energies vary by less than 0.02 eV compared with QCISD(T)/6-311++G**results from previous research by Zapata-Escobar et al.[36] implying that the present approach is fitting for analysis of larger clusters.

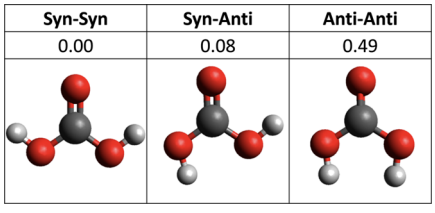


**Figure 1.** Monomer isomers with the relative energy in eV increasing from left to right.

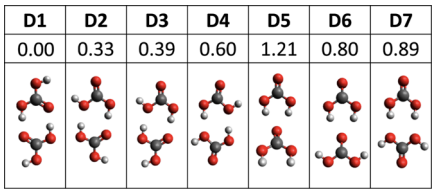


**Figure 2.** Dimer isomers explored in this work with the relative energy in eV increasing from left to right.

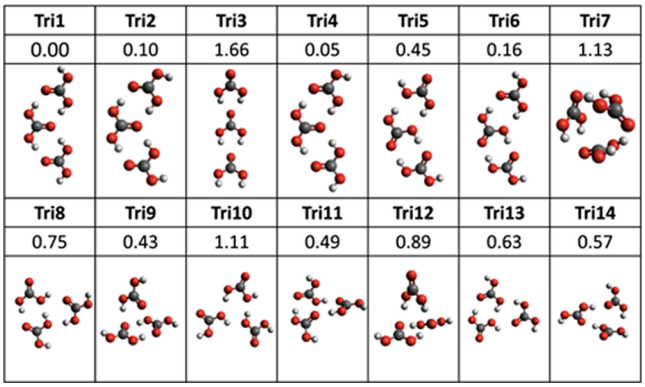


**Figure 3.** Trimer isomers with the relative energy in eV.

For dimers, the two *syn*−*syn* molecules engaging in hydrogen bonding have the lowest relative energy also in line with previous work.[35] This strong connection is due to two hydrogen bonds forming a hexagonal ring, while outside hydrogens remain in the *syn* position. Additionally, the molecules both lie flat on the same *xy*-plane due to the trigonal planar $sp^2$-hybridized carbon in the center of each molecule. One can compare the two *syn*−*anti* molecules, D3 and D4 from Figure 2, to show that hydrogen bonding with one H−O−C *syn* hydrogen is more energetically favorable than having both H−O−C *anti* hydrogens engaged in making the two hydrogen bonds. These observations support the *syn* position as the lowest energy form for hydrogen and ketone. Ultimately, the structures containing the *anti*−*anti* motif are all relatively high in energy.

The lowest relative energy for the trimer is a *syn*−*syn* molecule adding onto the D1 structure in Figure 2, which is the beginning of a ribbon structure. This ribbon structure is extended with more *syn*−*syn* molecules. At three molecules, three-dimensional isomers begin to arise; however, these are all higher in energy than the ribbon structure. Comparing the energies of Tri1, Tri2, and Tri3 in Figure 3, the cost of a *syn*−



https://doi.org/10.1021/acs.jpca.1c02878
J. Phys. Chem. A 2021, 125, 4589−4597

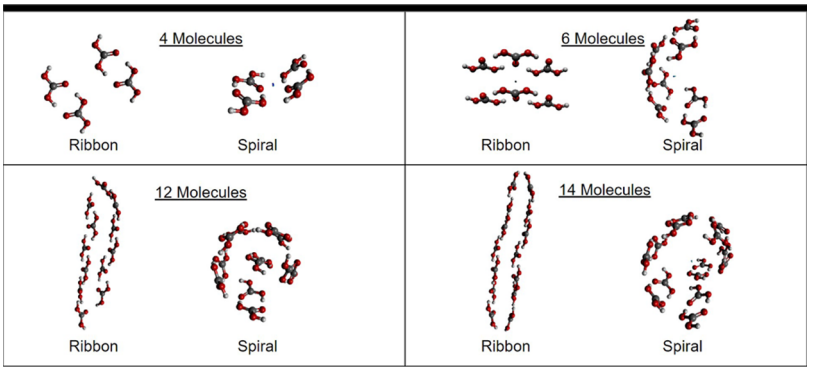


**Figure 4.** Stacked ribbon and spiral geometries.

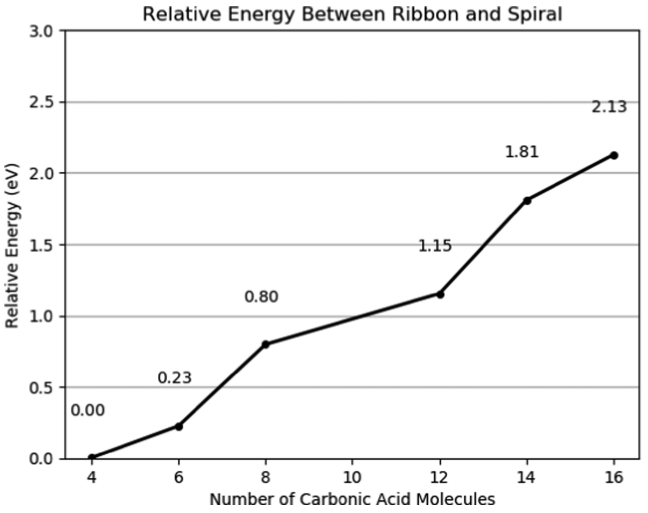


**Figure 5.** Relative energy (eV) between the ribbon and spiral structures according to ωB97XD/6-31+G*.

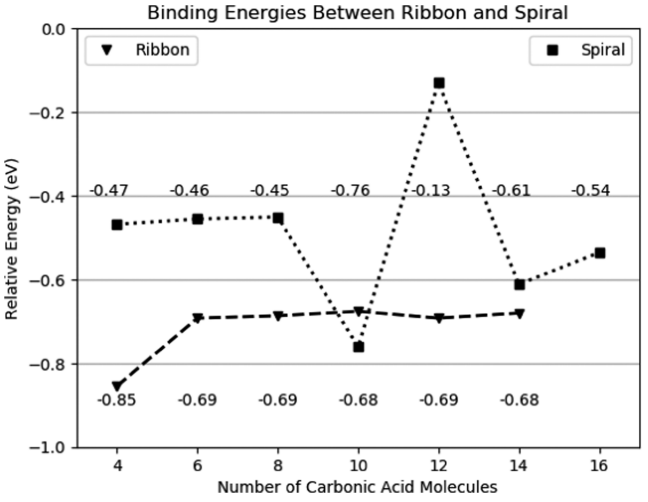


**Figure 6.** Binding energies for the spiral and ribbon with adding dimers.

*anti* molecule at the end of the ribbon is about 0.5 eV. When the *anti*−*anti* trimer completes a circuit as in Tri7, it becomes more stable compared to Tri3, albeit higher in intermolecular angular strain, since the hydrogens are all engaging in hydrogen bonding. This example highlights a pattern that when more hydrogens are unable to engage in hydrogen bonding, the relative energy increases significantly. Therefore, although the three-dimensional structures are higher in relative energy; these structures might become more favorable in a solid

**Table 1. Excited-State Data (eV) for the *syn*−*syn* Monomer**

| | EOM-CCSD/aug-cc-pVDZ | | B3LYP/6-311G(d,p) | | |
|---|---|---|---|---|---|
| excited state | exc. energy | *f* | exc. energy | *f* | energy difference |
| $1\ ^1A_1$ | 8.49 | 0.017 | 8.42 | 0.004 | 0.07 |
| $2\ ^1A_1$ | 9.28 | 0.222 | 9.70 | 0.165 | −0.42 |
| $1\ ^1B_1$ | 8.15 | 0.001 | 8.19 | 0.001 | −0.04 |
| $2\ ^1B_1$ | 10.10 | 0.053 | 9.99 | 0.016 | 0.11 |
| $1\ ^1B_2$ | 7.54 | 0.043 | 7.54 | 0.038 | 0.00 |
| $2\ ^1B_2$ | 9.72 | 0.001 | 10.05 | 0.161 | −0.33 |
| $1\ ^1A_2$ | 7.22 | 0.000 | 7.04 | 0.000 | 0.18 |

**Table 2. Excited-State Data (eV) for the Dimer**

| | EOM-CCSD/aug-cc-pVDZ | | B3LYP/6-311G(d,p) | | |
|---|---|---|---|---|---|
| excited state | exc. energy | *f* | exc. energy | *f* | energy difference |
| $1\ ^1A_g$ | 8.06 | 0.000 | 8.23 | 0.000 | −0.17 |
| $2\ ^1A_g$ | 8.74 | 0.000 | 8.75 | 0.000 | −0.01 |
| $1\ ^1A_u$ | 7.58 | 0.001 | 8.35 | 0.000 | −0.78 |
| $2\ ^1A_u$ | 8.46 | 0.001 | 8.69 | 0.001 | −0.23 |
| $1\ ^1B_u$ | 8.08 | 0.086 | 8.27 | 0.065 | −0.19 |
| $2\ ^1B_u$ | 9.11 | 0.303 | 9.57 | 0.322 | −0.46 |
| $1\ ^1B_g$ | 7.59 | 0.000 | 7.34 | 0.000 | 0.24 |

**Table 3. Excited-State Data (eV) for the Ribbon Tetramer**

| | EOM-CCSD/aug-cc-pVDZ | | B3LYP/6-311G(d,p) | | |
|---|---|---|---|---|---|
| excited state | exc. energy | *f* | exc. energy | *f* | energy difference |
| $1\ ^1A_g$ | 8.14 | 0.000 | 8.31 | 0.000 | −0.17 |
| $2\ ^1A_g$ | 8.66 | 0.000 | 8.77 | 0.000 | −0.11 |
| $1\ ^1A_u$ | 7.58 | 0.001 | 7.33 | 0.001 | 0.25 |
| $2\ ^1A_u$ | 7.93 | 0.000 | 8.26 | 0.000 | −0.33 |
| $1\ ^1B_u$ | 8.14 | 0.094 | 8.31 | 0.067 | −0.17 |
| $2\ ^1B_u$ | 8.76 | 0.031 | 9.51 | 0.073 | −0.75 |
| $1\ ^1B_g$ | 7.58 | 0.000 | 7.33 | 0.000 | 0.25 |



https://doi.org/10.1021/acs.jpca.1c02878
J. Phys. Chem. A 2021, 125, 4589−4597

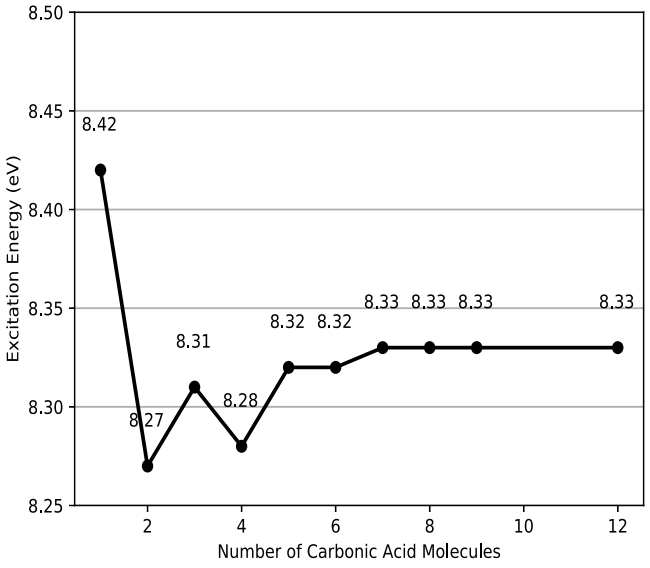


**Figure 7.** $^{1}B_{u}$ excitation energy for ribbons at 8.3 eV.

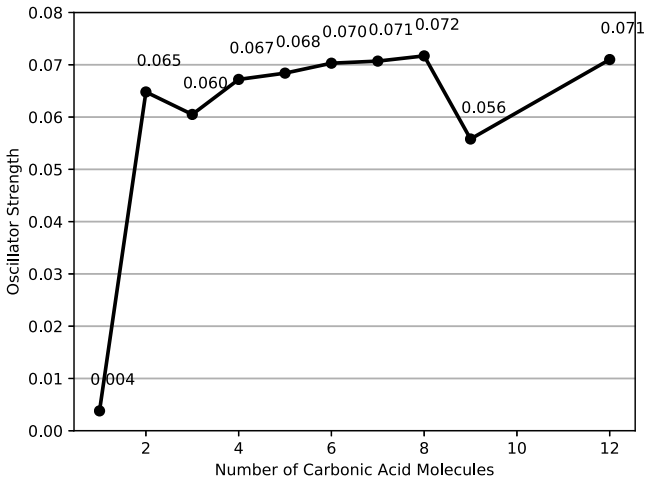


**Figure 8.** Associated oscillator strength for the $^{1}B_{u}$ excited state for ribbons at 8.3 eV.

structure where the noninteracting hydrogens on the outside no longer cause an increase in relative energy from not engaging in hydrogen bonding.

An exception to the *syn*−*syn* molecule being lower in energy than the *syn*−*anti* is found when comparing Tri11 and Tri14. These molecules engage in a similar pattern and exist in nearly

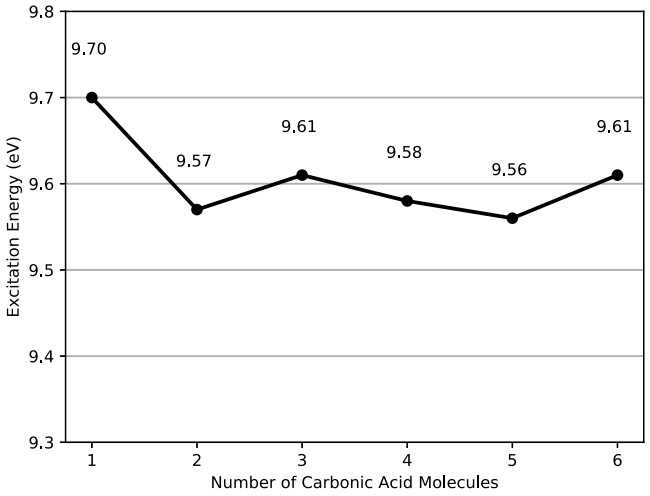


**Figure 10.** $^{2}B_{u}$ excitation energy for ribbons at 9.6 eV.

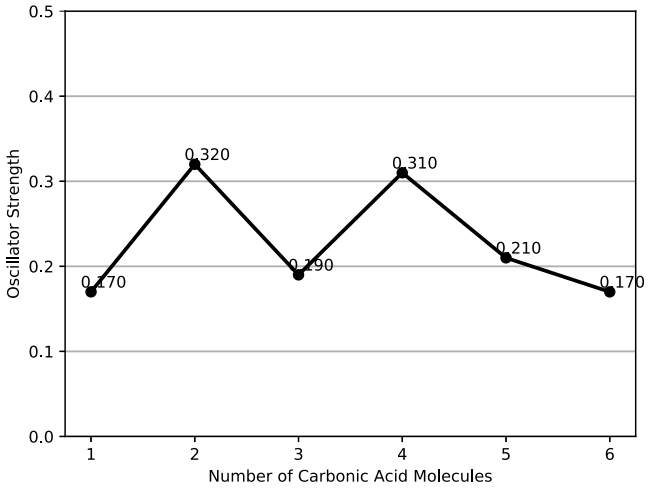


**Figure 11.** Associated oscillator strength for the $^{2}B_{u}$ excited state for ribbons at 9.6 eV.

the same space when overlapped. However, the Tri11 structure is about 0.75 eV lower in energy. In any case, as the ribbon motif is maintained going to larger clusters (i.e., longer ribbons) of carbonic acid dimers, the structures maintain $C_{2h}$ symmetry.

Further exploration of larger systems with more *syn*−*anti* and *anti*−*anti* molecules shows that the relative energies increase when the system is not comprised solely of the *syn*−

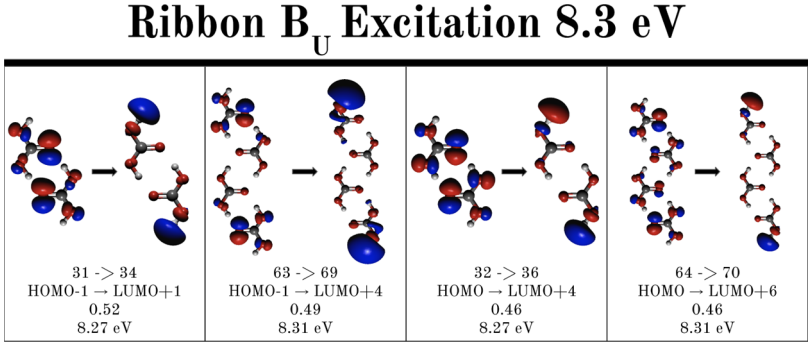


**Figure 9.** Molecular orbitals for the dimer and tetramer $^{1}B_{u}$ excitation around 8.3 eV are depicted here.



https://doi.org/10.1021/acs.jpca.1c02878
J. Phys. Chem. A 2021, 125, 4589−4597

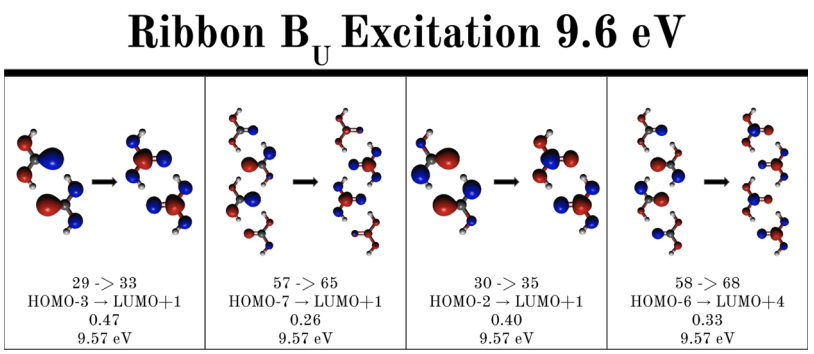


**Figure 12.** Molecular orbitals for the dimer and tetramer $^2B_u$ excitation around 9.6 eV are depicted here.

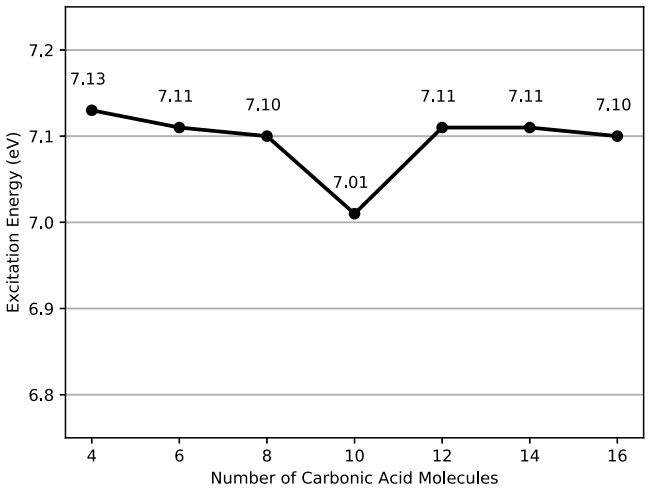


**Figure 13.** $^1B$ excitation energy for spirals at 7.1 eV.

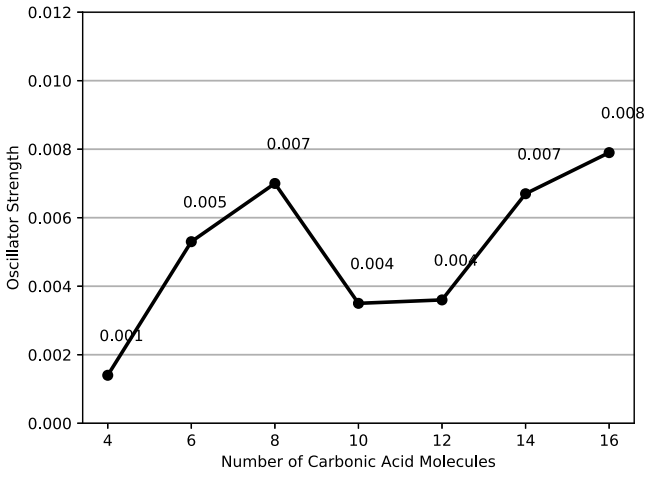


**Figure 14.** Associated oscillator strength for the $^1B$ excited state for spirals at 7.1 eV.

*syn* molecules. The supplemental information contains more isomers and relative energy figures for the tetramer and larger. From the dimer to dodecamer, *syn*−*syn* forms are the lowest relative energy, with the ensuing ribbon structure being the lowest isomeric form, until stacking two hexamer ribbons. The stacking of ribbons can be seen in Figure 4 and is the three-dimensional form of the ribbon structure. When stacking the ribbons, the tips of a ribbon bend toward the tips of the other ribbon, for example, the ribbon image of 12 molecules in Figure 4. Oxygens are puckering in an attempt to hydrogen bond with hydrogens present that lack a hydrogen bond interaction, and this is likely only an artifact of the present computations. The centers of the ribbons keep a distance of about 3.0 Å.

Another viable, three-dimensional *syn*−*syn* isomer is the spiral. The structure contains the most favorable *syn*−*syn* dimer, like the ribbon; however, instead of extending in one dimension, dimers engage in hydrogen bonding from the side. The spiral requires a minimum of four carbonic acid molecules in a slipped position with one rotated out of the plane by 40.4°, as shown in Figure 4. It maintains $C_2$ symmetry even as more dimers are added to the cluster in this motif. The spiral structure is inspired by Candidate V from previous work by Reddy et al.;[14] however, the geometry optimizations in the present study on such a molecular motif settled upon the ribbon structure. One complete spiral of the helix requires seven dimers—14 carbonic acid molecules.

These two main isomeric structures, the stacked ribbon and spiral, comprised of only the *syn*−*syn* molecules and extending in three dimensions are compared in relative energies and binding energies in Figures 5 and 6. The ribbon and spiral structures both have a strong hexagonal ring between adjacent *syn*−*syn* molecules. Hence, both have the lowest energy dimer formation within them, and the structures deviate from each other by the location where more dimers are added. Additionally, both the stacked ribbon and the spiral attempt to minimize the number of hydrogens not engaging in hydrogen bonding.

These two main isomeric structures, the stacked ribbon and spiral, comprising of only the *syn*−*syn* molecules and extending in three dimensions are compared in relative energies and binding energies in Figures 5 and 6. The ribbon and spiral structures both have the strong hexagonal ring between adjacent *syn*−*syn* molecules. Hence, both have the lowest energy dimer formation within them, and the structures deviate from each other by the location where more dimers are added. Additionally, both the stacked ribbon and the spiral attempt to minimize the number of hydrogens not engaging in hydrogen bonding. Comparing the relative energies of these two structures in Figure 5 shows the ribbon structure as the more favorable form since the consistent positive energy increase indicates favorability toward the stacked ribbon structure as the clusters become larger. Therefore, the binding energies for the ribbon structure are expected to be lower than that of the spiral.

From Figure 6, the stacked ribbon and spiral binding energies behave differently. The ribbon's binding energy approaches a constant value around −0.75 eV for every


https://doi.org/10.1021/acs.jpca.1c02878
J. Phys. Chem. A 2021, 125, 4589−4597

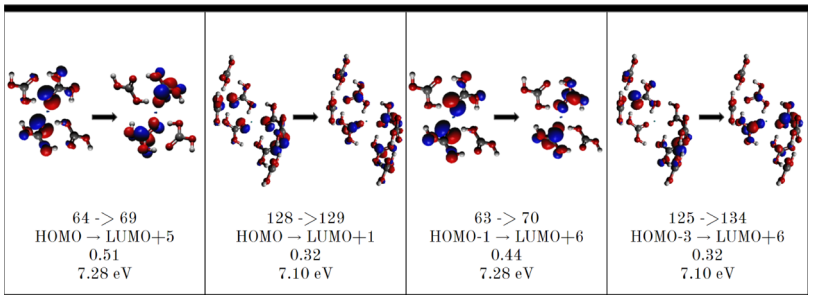


**Figure 15.** Molecular orbitals for the tetramer and octamer spiral structure $^1$B excitation are shown here.

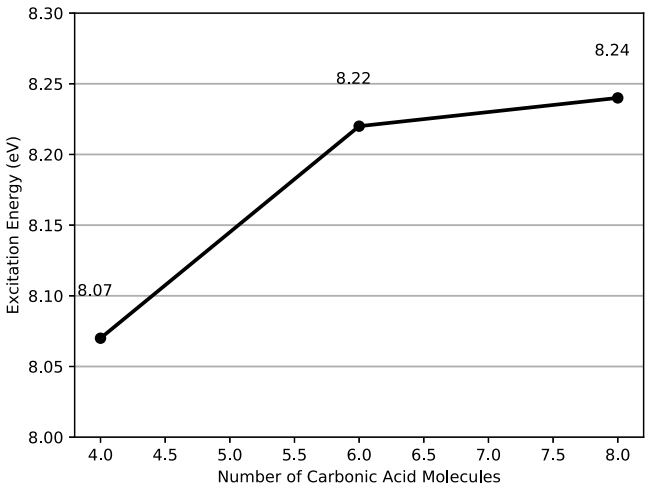


**Figure 16.** $^1$B excitation energy for spirals at 8.1 eV.

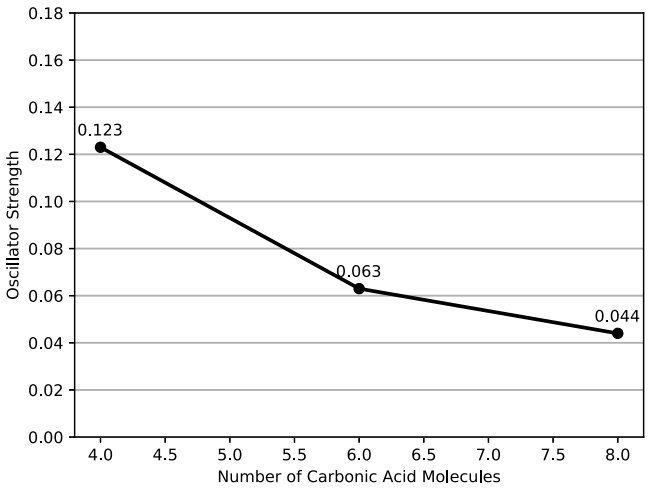


**Figure 17.** Associated oscillator strength for the $^1$B excited state for spirals at 8.1−8.2 eV.

dimer added past 6 total carbonic acid molecules in the cluster. The spiral has two regions with a slight trend upwards separated by a discrepancy at the decamer and dodecamer. This discrepancy is the energy manifestation of the spiral helix being one dimer away from making a complete circulation. Ultimately, the stacked ribbon structure is more favorable in energy than the spiral structure as the cluster grows in size because the ribbon's average binding energy is −0.71 eV, while the spiral's average binding energy is −0.70 eV. Consequently, the ribbon will decrease in energy at a faster rate than the spiral when extending the size of the cluster.

**Excitation Energies.** *Ribbon Excitation Energies.* The electronic excitations for carbonic acid clusters of both ribbon and spiral motifs are calculated and their molecular orbitals plotted to aid in characterizing how the excitation energies shift as the cluster sizes increase toward the bulk. Additionally, the energies between the EOM-CCSD/aug-cc-pVDZ and the B3LYP/6-311G(d,p) excited-state calculations are compared through tables and spectral graphs of the ribbon monomer, dimer, tetramer, and spiral tetramer resulting in a mean absolute difference of 0.18 eV.

The *syn*−*syn* monomer has an excited state at 9.28 eV with the highest oscillator strength (*f*) of 0.22 (Table 1). This *f* value is much larger than the other noticeable excitations at 10.10 eV with an *f* of 0.053 and at 7.54 eV with an *f* of 0.043. The B3LYP/6-311G(d,p) and EOM-CCSD/aug-cc-pVDZ calculations vary by about ±0.5 eV with the EOM-CCSD calculation likely providing a more accurate number.[37] For instance, EOM-CCSD computes the second 1 $^1$A$_1$ to be 9.28 eV, while B3LYP is 9.70 eV with a −0.42 eV difference.

Next, Table 2 shows the excited states for the most stable dimer from Figure 2. The most noticeable excited states are both $^1$B$_u$ with the EOM-CCSD energies of 8.08 and 9.11 eV with the respective oscillator strengths of 0.086 and 0.303. These values differ from the B3LYP/6-311G(d,p) energies by less than 0.5 eV with the lower energy value at 8.27 eV and the higher energy point at 9.57 eV for TD-DFT computations. The relatively large *f* value on the $^1$B$_u$ 9.11 eV excitation likely produces a detectable signal.

In Table 3, excited states for the lowest energy form of the ribbon tetramer are displayed. Once again the EOM-CCSD/aug-cc-pVDZ values for two of the $^1$B$_u$ excitations are around the same energies as the TD-DFT excited states, although *f* decreases. The lower energy value for the EOM-CCSD calculation reports excitations at 8.14 and 8.76 eV with the oscillator strengths of 0.093 and 0.031, respectively. These relate to the B3LYP energies of 8.31 and 9.51 eV. From these points, a trend is starting to emerge with the increase of the ribbon's size having negligible effects on excitation energies. Figure S3 depicts this data visually on an absorption plot. Since the systems start to become too costly to run EOM-CCSD/aug-cc-pVDZ, the electronically excited states of larger ribbon structures are calculated with only B3LYP/6-311G(d,p).

In Figure 7, the $^1$B$_u$ excitation energy for ribbon clusters around 8.3 eV are displayed. Excluding the monomer, excitation energies are approaching an asymptote at 8.37 eV, while the oscillator strength stays approximately the same after seven carbonic acid molecules are in the cluster, as shown in Figure 8. However, to ensure that these excitations are the same excitation throughout the polymers, the orbitals are


https://doi.org/10.1021/acs.jpca.1c02878
J. Phys. Chem. A 2021, 125, 4589−4597

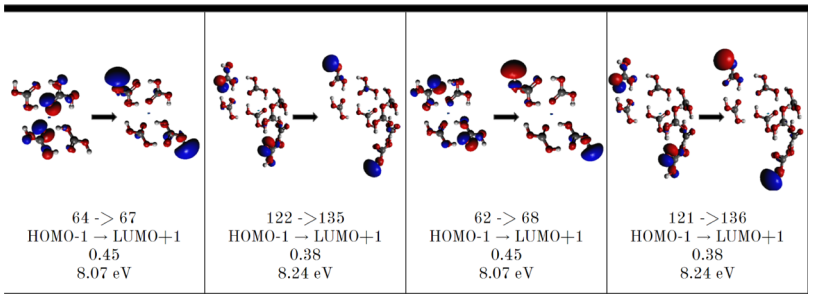


**Figure 18.** Molecular orbitals for the tetramer and octamer spiral structure $^1$B excitation are shown here.

plotted in Figure 9. Comparing the highest contributors of the dimer to ribbon tetramer excitations in Figure 9, the orbitals are what would be expected for similar excitations in more distributed systems. The most notable excited state for the dimer is the $^1B_u$ state at 8.27 eV and is comprised of molecular orbital (MO) contributions from an in-plane $\pi$ orbital to a $\sigma^*$ MO with a character of 0.52. These orbitals are the HOMO − 1 and the LUMO + 1. This behavior is mimicked in the ribbon tetramer $^1B_u$ excitation at 8.31 eV from the HOMO − 1 and the LUMO + 4; however, the in-plane $\pi$ orbital is centralized on the ending two carbonic acid molecules. This has a 0.49 character of the excited state making it the largest contributor. Looking at the second-highest contributors, the dimer and ribbon tetramer have another in-plane $\pi$ to a $\sigma^*$ excitation. However, the in-plane $\pi$ orbital is distributed across all of the molecules in the dimer and tetramer alike. This contribution for dimer and ribbon tetramer is 0.49 and 0.46, respectively. Overall, the energy difference between the dimer and tetramer excitations is 0.04 eV and increases from the dimer to tetramer, but these are the same type of excitation.

Then, the tetramer ribbon and the hexamer ribbon excitation around 8.3 eV are compared. The tetramer excitations described above are similar to the two, corresponding $^1B_u$ excitations from the hexamer, with excitation energy for the hexamer at 8.32 eV, a 0.01 eV increase. The contributions are 0.48 for the HOMO − 3 to LUMO + 5 and 0.46 from the HOMO − 2 to the LUMO + 6. These contributions are in very close agreement with the tetramer. After analyzing the orbitals for the octamer and dodecamer as well, Figure 7 is depicting the same type of excitation.

Figures 10−12 depict a similar analysis to the excited state described above; however, the $^1B_u$ excitation around 9.6 eV for ribbons is investigated. From Figure 10, extrapolation of the points appears to give an asymptotic convergence to around 9.70 eV as the number of carbonic acids approaches the bulk. Additionally, the oscillator strength seems to be dampening toward a constant value between 0.2 and 0.3 as the system becomes larger.

The molecular orbitals are displayed in Figure 12 to determine if the excitations are similar. For the dimer $^1B_u$ excitation, the energy is 9.57 eV and is an out-of-plane, in-phase $\pi$ to out-of-plane, in-phase $\pi^*$ excitation. The dimer excited state is the HOMO − 3 to LUMO + 1. This description matches the highest contributor of the ribbon tetramer's $^1B_u$ excitation at 9.57 eV from HOMO − 7 to LUMO + 1. The contributions from the dimer and tetramer are 0.47 and 0.26. The second-highest contributors are out-of-phase, out-of-plane $\pi$ to out-of-phase, out-of-plane $\pi^*$ $^1B_u$ excitation. These contributions are 0.40 and 0.33. Therefore, these two excitations are of the same type.

Moving on to the larger systems for comparison, the hexamer has a $^1B_u$ excitation energy of 9.61 eV. The tetramer HOMO − 7 to LUMO + 1 orbitals involved in the excitation match that of the hexamer HOMO − 11 to LUMO + 1 orbitals and has a contribution of 0.13. Meanwhile, the tetramer HOMO − 6 to LUMO + 3 excitation matches the largest contributor of the hexamer of orbital 86 to 100—HOMO − 10 to LUMO + 3—with the contribution of 0.24. For this $^1B_u$ excitation, contributions from more orbitals increase with the carbonic acid molecules present. Therefore, although these contributions seem small, they are still the largest contributors to the excitation. Overall, these $^1B_u$ excited states are around the same energy with the addition of many carbonic acid molecules.

*Spiral Excitation Energies.* Then, the spiral tetramer structure has a $^1$B excited state with an energy and oscillator strength of 7.36 eV and 0.001 for EOM-CCSD/aug-cc-pVDZ and 7.13 eV and 0.001 for B3LYP/6-311G(D,p). These energies differ by 0.23 eV. This is the only spiral oligomer that has both EOM-CCSD/aug-cc-pVDZ and B3LYP/6-311G(d,p) excitation energies due to the costs of the EOM-CCSD calculation. The plotted molecular orbitals both have a large contribution from an in-plane $\pi$ to out-of-plane $\pi^*$ excitation.

For spiral excitations, Figures 13 and 14 plot the excitation energy and $f$ of the $^1$B excitation around 7.1 eV. Except for the dip at 10 molecules, the spiral has an excitation that decreases slowly to a value around 7.1 eV. The $f$ starts very weak, but increases slightly as the structure becomes larger.

The molecular orbitals in Figure 15 show that these excitations are the same as the structure increases. The major contributors are, again, both in-plane $\pi$ to out-of-plane $\pi^*$ excitation. For the tetramer, orbital excitations are from the HOMO to LUMO + 4 with a 0.51 contribution and HOMO − 1 to LUMO + 5 with a contribution of 0.44. The larger contributor's excited state is from the HOMO to the LUMO + 4, and the second-highest contributor is the HOMO − 1 to the LUMO + 5. For the octamer, major contributors are the HOMO to the LUMO and the HOMO − 4 to LUMO + 6 both with the respective excitation characters of 0.32.

Finally, the last notable excitation in the spiral is around 8.1−8.2 eV. Figure 16 shows an upward trend in energy as the structure increases in size; meanwhile, the $f$ decreases as shown in Figure 17. From Figure 18, the molecular orbitals that are largely responsible for this excitation both start in an in-plane $\pi$ orbital and end in a $\sigma^*$ orbital; however, in both instances, the phases are different. The tetramer larger contributor is from orbital 64 to 67—HOMO to the LUMO + 2—with 0.45, while


https://doi.org/10.1021/acs.jpca.1c02878
J. Phys. Chem. A 2021, 125, 4589−4597

the second contributor is from orbital 62 to 68—HOMO − 2 to LUMO + 3—with 0.45 as well. Within the octamer, the larger contributor that lines up with the tetramer is from orbital 122 to 135—HOMO − 6 to LUMO + 6—with 0.38 and the second contributor is from orbital 121 to 136—HOMO − 7 to LUMO + 7—with 0.38.

## CONCLUSIONS

A new motif for the early clustering of carbonic acid incorporates the lowest energy dimer into a spiral or helical pattern. While this structural behavior is not the most energetically favorable when compared to the ribbon (or linear) motif, this novel arrangement of carbonic acid molecules costs roughly only about 0.2 eV of energy for each dimer unit added. Furthermore, the helical oligomerization is chiral and would induce optical activity in any incident light interacting with such material. This chirality combined with the importance and ubiquity of the constituent water and carbon dioxide molecules implies that the helical spiral motif of carbonic acid may have implications for astrobiology and origins of life studies, especially in evaporation studies of photoprocessed astrophysical ices. Laboratory differentiation of these motifs is likely straightforward with the helical spiral structure absorbing at lower UV energies (<8.1 eV) and the linear, ribbon form absorbing at higher energies (>8.1 eV). Ultimately, these data should assist in detecting small clusters of carbonic acid as they begin to nucleate in various extended systems.

## AUTHOR INFORMATION


### Corresponding Author

**Ryan C. Fortenberry** − *Department of Chemistry & Biochemistry, University of Mississippi, University, Mississippi 38677-1848, United States;* orcid.org/0000-0003-4716-8225; Email: r410@olemiss.edu

### Author

**Austin M. Wallace** − *Department of Chemistry & Biochemistry, University of Mississippi, University, Mississippi 38677-1848, United States*

Complete contact information is available at: https://pubs.acs.org/10.1021/acs.jpca.1c02878


### Notes

The authors declare no competing financial interest.

## ACKNOWLEDGMENTS

The authors acknowledge funding from NSF Grant OIA-1757220 and Startup Funds provided by the University of Mississippi as well as computing support from the Mississippi Center for Supercomputing Research. The authors also wish to acknowledge Prof. Ralf I. Kaiser of the University of Hawaii and Prof. Sergio Ioppolo of Queen Mary University of London for discussions related to this project. Finally, AMW wishes to thank the Barry Goldwater Scholarship and Excellence in Education Foundation for support of his research.

## REFERENCES


(1) Strazzulla, G.; Brucato, J. R.; Palumbo, M. E. Carbonic Acid on Mars. *Planet. Space Sci.* **1996**, *44*, 1447−1450.

(2) Zheng, W.; Kaiser, R. I. On the Formation of Carbonic Acid ($H_2CO_3$) in Solar System Ices. *Chem. Phys. Lett.* **2007**, *450*, 55−60.

(3) Jones, B. M.; Kaiser, R. I.; Strazzulla, G. Carbonic Acid as a Reserve of Carbon Dioxide on Icy Moons: The Formation of Carbon Dioxide ($CO_2$) in a Polar Environment. *Astrophys. J.* **2014**, *788*, No. 170.

(4) Radhakrishnan, S.; Gudipati, M. S.; Sander, W.; Lignell, A. Photochemical Processes in $CO_2/H_2O$ Ice Mixtures with Trapped Pyrene, a Model Polycyclic Aromatic Hydrocarbon. *Astrophys. J.* **2018**, *864*, No. 151.

(5) Sandford, S. A.; Nuevo, M.; Bera, P. P.; Lee, T. J. rebiotic Astrochemistry and the Formation of Molecules of Astrobiological Interest in Interstellar Clouds and Protostellar Disks. *Chem. Rev.* **2020**, *120*, 4616−4659.

(6) Moore, M. H.; Khanna, R. K. Infrared and Mass Spectral Studies of Proton Irradiated $H_2O$ + $CO_2$ Ice: Evidence for Carbonic Acid. *Spectrochim. Acta, Part A* **1991**, *47*, 255−262.

(7) Peeters, Z.; Hudson, R.; Moore, M.; Lewis, A. The Formation and Stability of Carbonic Acid on Outer Solar System Bodies. *Icarus* **2010**, *210*, 480−487.

(8) Ioppolo, S.; Kanuchová, Z.; James, R. L.; Dawes, A.; Ryabov, A.; Dezalay, J.; Jones, N. C.; Hoffmann, S. V.; Mason, N. J.; Strazzulla, G. Vacuum Ultraviolet Photoabsorption Spectroscopy of Space-Related Ices: Formation and Destruction of Solid Carbonic Acid upon 1 keV Electron Irradiation. *Astron. Astrophys.* **2021**, *646*, No. A172.

(9) Bernard, J.; Seidl, M.; Kohl, I.; Liedl, K. R.; Mayer, E.; Gálvez, Ó.; Grothe, H.; Loerting, T. Spectroscopic Observation of Matrix-Isolated Carbonic Acid Trapped from the Gas Phase. *Angew. Chem., Int. Ed.* **2011**, *50*, 1939−1943.

(10) Mitterdorfer, C.; Bernard, J.; Klauser, F.; Winkel, K.; Kohl, I.; Liedl, K. R.; Grothe, H.; Mayer, E.; Loerting, T. Local Structural Order in Carbonic Acid Polymorphs: Raman and FT-IR Spectroscopy. *J. Raman Spectrosc.* **2012**, *43*, 108−115.

(11) Bernard, J.; Huber, R. G.; Liedl, K. R.; Grothe, H.; Loerting, T. Matrix Isolation Studies of Carbonic Acid-The Vapor Phase above the $\beta$-Polymorph. *J. Am. Chem. Soc.* **2013**, *135*, 7732−7737.

(12) Köck, E.; Bernard, J.; Podewitz, M.; Dinu, D. F.; Huber, R. G.; Liedl, K. R.; Grothe, H.; Bertel, E.; Schlögl, R.; Loerting, T. Alpha-Carbonic Acid Revisited: Carbonic Acid Monomethyl Ester as a Solid and Its Conformational Isomerism in the Gas Phase. *Chem. - Eur. J.* **2020**, *26*, 285−305.

(13) Reddy, S.; Balasubramanian, S. Carbonic Acid: Molecule, Crystal and Aqueous Solution. *Chem. Commun.* **2013**, *50*, 503−514.

(14) Reddy, S.; Chidambar, H.; Balasubramanian, S. Theoretical Investigations of Candidate Crystal Structures for $\beta$-Carbonic Acid. *J. Chem. Phys.* **2011**, *134*, No. 124511.

(15) Chai, J.-D.; Head-Gordon, M. Systematic Optimization of Long-Range Corrected Hybrid Density Functionals. *J. Chem. Phys.* **2008**, *128*, No. 084106.

(16) Chai, J.-D.; Head-Gordon, M. Long-range Corrected Hybrid Density Functionals With Damped Atom-Atom Dispersion Corrections. *Phys. Chem. Chem. Phys.* **2008**, *10*, 6615−6620.

(17) Clark, T.; Chandrasekhar, J.; Spitznagel, G.; Schleyer, P. Efficient Diffuse Function-Augmented Basis Sets for Anion Calculations. III. The 3-21+G Basis Set for First-Row Elements, Li-F. *J. Comput. Chem.* **1983**, *4*, 294−301.

(18) Ditchfield, R.; Hehre, W. J.; Pople, J. A. Self-Consistent Molecular-Orbital Methods. IX. An Extended Gaussian-Type Basis for Molecular-Orbital Studies of Organic Molecules. *J. Chem. Phys.* **1971**, *54*, 724−728.

(19) Hariharan, P. C.; Pople, J. A. The Influence of Polarization Functions on Molecular Orbital Hydrogenation Energies. *Theor. Chim. Acta* **1973**, *28*, 213−222.

(20) Hehre, W. J.; Ditchfield, R.; Pople, J. A. Self-Consistent Molecular Orbital Methods. XII. Further Extensions of Gaussian-Type Basis Sets for Use in Molecular Orbital Studies of Organic Molecules. *J. Chem. Phys.* **1972**, *56*, 2257−2261.

(21) Frisch, M. J.; Trucks, G. W.; Schlegel, H. B.; Scuseria, G. E.; Robb, M. A.; Cheeseman, J. R.; Scalmani, G.; Barone, V.; Petersson, G. A.; Nakatsuji, H.; et al. *Gaussian 16*, revision C.01; Gaussian Inc.: Wallingford, CT, 2016.

(22) Karamanis, P. The Importance of the DFT Method on the Computation of the Second Hyperpolarizability of Semiconductor Clusters of Increasing Size: A Critical Analysis on Prolate Aluminum Phospide Clusters. *Int. J. Quantum Chem.* **2011**, *112*, 2115−2125.
(23) Adamo, C.; Jacquemin, D. The Calculations of Excited-State Properites with Time-Dependent Density Functional Theory. *Chem. Soc. Rev.* **2013**, *42*, No. 845.
(24) Laurent, A. D.; Adamo, C.; Jacquemin, D. Dye Chemistry with Time-Dependent Density Functional Theory. *Phys. Chem. Chem. Phys.* **2014**, *16*, 14334−14356.
(25) Becke, A. D. Density-Functional Thermochemistry. III. The Role of Exact Exchange. *J. Chem. Phys.* **1993**, *98*, 5648−5652.
(26) Yang, W. T.; Parr, R. G.; Lee, C. T. Various Functionals for the Kinetic Energy Density of an Atom or Molecule. *Phys. Rev. A* **1986**, *34*, 4586−4590.
(27) Lee, C.; Yang, W. T.; Parr, R. G. Development of the Colle-Salvetti Correlation-Energy Formula into a Functional of the Electron Density. *Phys. Rev. B.* **1988**, *37*, 785−789.
(28) Krishnan, R.; Binkley, J.; Seeger, R.; Pople, J. A. Self-Consistent Molecular Orbital Methods. XX. A Basis Set for Correlated Wave Functions. *J. Chem. Phys.* **1980**, *72*, 650−654.
(29) Krylov, A. I. Equation-of-Motion Coupled Cluster Methods for Open-Shell and Electronically Excited Species: The Hitchikeras Guide to Fock Space. *Annu. Rev. Phys. Chem.* **2007**, *59*, 433−463.
(30) Shavitt, I.; Bartlett, R. J. *Many-Body Methods in Chemistry and Physics: MBPT and Coupled-Cluster Theory*; Cambridge University Press: Cambridge, 2009.
(31) Stanton, J. F.; Bartlett, R. J. The Equation of Motion Coupled-Cluster Method—A Systematic Biorthogonal Approach to Molecular Excitation Energies, Transition-Probabilities, and Excited-State Properties. *J. Chem. Phys.* **1993**, *98*, 7029−7039.
(32) Werner, H.-J.; Knowles, P. J.; Knizia, G.; Manby, F. R.; Schütz, M.; Celani, P.; Györffy, W.; Kats, D.; Korona, T.; Lindh, R.; et al. *MOLPRO, version 2019.2, A Package of Ab Initio Programs*, 2019. http://www.molpro.net.
(33) Kendall, R. A.; Dunning, T. H.; Harrison, R. J. Electron Affinities of the First-Row Atoms Revisited. Systematic Basis Sets and Wave Functions. *J. Chem. Phys.* **1992**, *96*, 6796−6806.
(34) Dunning, T. H. Gaussian Basis Sets for Use in Correlated Molecular Calculations. I. The Atoms Boron through Neon and Hydrogen. *J. Chem. Phys.* **1989**, *90*, 1007−1023.
(35) Murillo, J.; David, J.; Restrepo, A. Insights into the Structure and Stability of the Carbonic Acid Dimer. *Phys. Chem. Chem. Phys.* **2010**, *12*, 10963−10970.
(36) Zapata-Escobar, A. D.; Murillo-López, J. A.; Hadad, C.; Restrepo, A. Understanding the Nature of Bonding Interactions in the Carbonic Acid Dimers. *J. Mol. Model.* **2019**, *25*, No. 20.
(37) Peters, W. K.; Couch, D. E.; Mignolet, B.; Shi, X.; Nguyen, Q. L.; Fortenberry, R. C.; Schlegel, H. B.; Remacle, F.; Kapteyn, H. C.; Murnane, M. M.; et al. Ultrafast 25 fs Relaxation in Highly Excited States of Methyl Azide Mediated by Strong Non-Adiabatic Coupling. *Proc. Nat. Acad. Sci. U.S.A.* **2017**, *114*, E11072−E11081.


https://doi.org/10.1021/acs.jpca.1c02878
*J. Phys. Chem. A* 2021, 125, 4589−4597